Journal of Fluids and Structures 120 (2023) 103896

Contents lists available at ScienceDirect

Journal of Fluids and Structures

journal homepage: www.elsevier.com/locate/jfs

Stability analysis for internal flow-induced vertical cantilevered pipe subject to multiple lumped masses

Yongqi Ma [a,d], Dingchang Zhou [a,c], Yunxiang You [a,b,c], Yijun Shen [d], Ke Chen [a,b,c], Aichun Feng [a,b,c,*]

[a] School of Naval Architecture, Ocean and Civil Engineering, Shanghai Jiao Tong University, Shanghai 200240, China
[b] State Key Laboratory of Ocean Engineering, Shanghai Jiao Tong University, Shanghai 200240, China
[c] Shanghai Jiao Tong University Yazhou Bay Institute of Deepsea Technology, Sanya 572000, China
[d] State Key Laboratory of Marine Resource Utilization in South China Sea, Hainan University, Haikou 570228, China

ARTICLE INFO

Article history:
Received 31 December 2022
Received in revised form 20 April 2023
Accepted 24 April 2023
Available online 9 May 2023

Keywords:
Stability analysis
Cantilevered pipe
Lumped masses
Harmonic differential quadrature (HDQ) method

ABSTRACT

This study investigates the effects of both single and multiple lumped masses attached to a vertical cantilevered pipe conveying internal flow. By introducing delta and Heaviside functions, the governing equation of the vibration of a pipe with lumped masses is newly established based on Hamilton's principle. The gravitational force of the lumped mass should be considered in the theoretical model but has been essentially ignored in previous research. The harmonic differential quadrature (HDQ) method is applied to solve the governing vibration equation. The newly developed model is validated through a comparison with published data. Numerical results show that the gravity force of the lumped mass plays an important role, and ignoring this force leads to inaccurate results in the investigation of lumped mass effects. The instability of the pipe is analyzed using this new model with various lumped mass weights, positions, and fluid mass ratios. The numerical results showed that lumped masses significantly affect the critical flow velocity, vibration frequency, and modal shapes. The conclusions are expected to supply valuable guidance to reduce pipe vibration using lumped masses in engineering applications.

1. Introduction

The cantilevered pipe is widely employed in fields such as deep sea mining, ocean thermal energy conversion (OTEC), solution mining, the oil and gas industries, and nuclear reactor systems (Paidoussis, 2014, 2016; Li and Yang, 2017; Liang et al., 2018; Balkaya and Kaya, 2021; Zhen and Zou, 2022; Hisamatsu and Utsunomiya, 2023). A vertical cantilevered pipe conveying fluid experiences flutter instability as the internal flow velocity reaches critical value. The vibration induces accidents such as fatigue failures, damage, and explosions. Hence, many researchers have performed stability analyses for internal flow-induced pipe vibration (Paidoussis, 1970; Kuiper and Metrikine, 2005; Paidoussis, 2008; Kuiper and Metrikine, 2008; Rinaldi and Paidoussis, 2010; Kheiri and Paidoussis, 2015; Butt et al., 2021; Bahaadini et al., 2018; Li et al., 2018; Askarian et al., 2020; Paidoussis, 2022).

A vertical cantilevered pipe can be used in deep-sea mining system to transport a mixture of water and nodules from the seabed to a mining vessel platform. Then, the processed ore debris and seawater are discharged into the ocean through

* Corresponding author at: School of Naval Architecture, Ocean and Civil Engineering, Shanghai Jiao Tong University, Shanghai 200240, China.
E-mail address: fengaichun@sjtu.edu.cn (A. Feng).

https://doi.org/10.1016/j.jfluidstructs.2023.103896
0889-9746/

Nomenclature

Abbreviation

DQ	Differential quadrature
DTM	Differential transformation method
FEM	Finite element method
HDQ	Harmonic differential quadrature

Symbols

$A_{ij}^{(n)}$	Weighting coefficients in n-order
D_o	External diameter of pipe
D_i	Internal diameter of pipe
$\boldsymbol{E}$	Matrix
EI	Bending stiffness
$f(x)$	Continuous function
g	Gravitational acceleration
$\boldsymbol{H}_{ij}$, $\boldsymbol{S}_{ij}$	Coefficient matrix
$H()$	Heaviside function
$\boldsymbol{I}$, $\boldsymbol{0}$	Identity and Null matrix
i, j, k,	Indices
i	Imaginary unit
K_k	The k-th dimensionless lumped mass ratio
L	Total pipe Length
x_k	Distance from the fixed end to the lumped mass
$\boldsymbol{M}$, $\boldsymbol{C}$, $\boldsymbol{K}$	Mass, damping and Stiffness matrix
m_f, m_p	Mass of the fluid and pipe per unit length
m_i	Lumped mass
N	Total grid points
t	Time
T, V	The pipe kinetic and strain energy
U	Internal flow velocity
u	Dimensionless flow velocity
u_{cr}	Dimensionless critical flow velocity
$w(x,t)$	Lateral displacement
x	Axial spatial variable

Greek symbols

γ	Dimensionless gravity
β	Dimensionless fluid mass ratio
Δ	Dimensionless displacement
δ	Small element of the pipe
$\delta()$	Dirac delta function
η	Dimensionless lateral deflection
λ	System eigenvalue
ξ	Dimensionless axial spatial variable
ζ_k	Length of lumped mass from fixed end
ρ_p, ρ_f	Density of pipe and fluid
σ	Dimensionless external damping parameter
τ	Dimensionless time
Ω	Eigenvalue
Ω_{cr}	Critical frequency
$\mathrm{Re}(\Omega)$, $\mathrm{Im}(\Omega)$	Real and imaginary part of eigenvalue

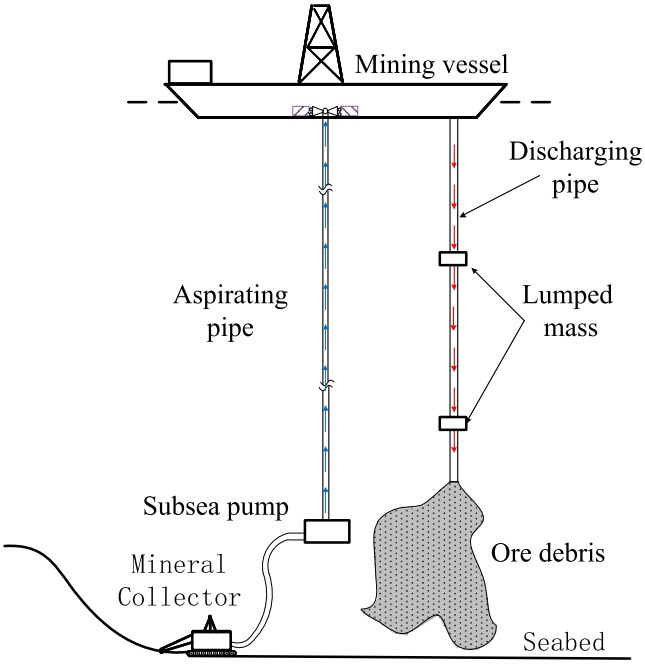

Fig. 1. Sketch of a deep-sea mining system.

a discharging pipe, as shown in Fig. 1. However, the discharged ore debris carries a large number of microbial communities. When the discharging pipe is too short (less than 200 m in length), it causes the death of microbial communities as a result of habitat changes or extinction of surrounding marine species groups, and thus destroys the original ecosystem. The discharging ore debris produces sediment clouds in the ocean, and these clouds may contain toxic heavy metals and may spread over long distances, disturbing the seabed and damaging the habitats of marine organisms. Furthermore, the discharging ore debris can affect the migration of marine fish. Therefore, the length of the discharging pipe should extend as far as possible to reach the seabed (pipe length greater than 1000 m) to minimize pollution of the ocean environment. To achieve this, it is necessary to study the vibration problem of long vertical discharging pipes. In order to avoid harmful vibrations, the pipe's critical flow velocity is usually designed to be as high as possible. The lumped mass may change the pipe's critical flow velocity significantly, and attaching a lumped mass has proven to be a very economical solution in practical applications. These facts spur research aiming to control pipe stability performance using lumped masses.

Hill and Swanson (1970) used theoretical and experimental methods to study the effects of adding lumped masses to a horizontal cantilevered pipe conveying fluid. The results showed that adding lumped masses reduced the critical flow velocity. Copeland and Moon (1992) used an experimental method to study the three-dimensional nonlinear dynamics of a cantilevered pipe conveying fluid with an end mass attached at the free end. Their experimental results revealed that the cantilevered pipe with an end mass exhibited quasi-periodic and chaotic motion as the flow further increased beyond the flutter instability, and suggested complex interactions between several unstable modes. Addessi et al. (2005) studied the in-plane free vibration of highly flexural beams with lumped masses and summarized the occurrence of modal steering phenomena. Yoon and Son (2007) investigated the dynamic stability of a rotating cantilevered pipe conveying fluid with a tip mass and found that the tip mass significantly affected pipe stability. Modarres-Sadeghi et al. (2007) and Wadham-Gagnon and Paidoussis (2013) investigated the three-dimensional nonlinear dynamics of a cantilevered pipe conveying fluid with an end mass attached at the free end using theoretical and experimental methods. They found that the resulting periodic motion followed a period-doubling or quasi-periodic path into chaos as the flow increased, depending on the end mass parameters. Fazelzadeh and Kazemi-Lari (2013) investigated the stability of a cantilevered pipe resting on an elastic foundation subject to a partially distributed follower force with a lumped mass located in an arbitrary position. It was found that the vibration amplitudes could be reduced by changing the position and weight of the lumped mass. Zhang et al. (2016) established nonlinear equations of three-dimensional motion for a horizontal cantilevered pipe conveying fluid with lumped masses at arbitrary positions along the pipe. It was found that the nonlinear vibration gradually evolved into three different forms as flow velocity increased: periodic motion, quasi-periodic motion, and chaotic motion. Na et al. (2019) examined the dynamic stability characteristics of liquid-filled cylindrical shells with lumped masses under a follower force, and found that the lumped mass, filling ratio, length ratio, and thickness ratio influenced the dynamic characteristics of the liquid-filled cylindrical shells. ElNajjar and Daneshmand (2020) studied the dynamical behavior of both horizontal and vertical cantilevered pipes conveying fluid with lumped masses and spring

elements. It was found that the critical flow velocity decreased for all fluid mass ratios for a pipe with two lumped masses located in the middle and at the end. Khudayarov et al. (2020) considered the vibration problems of a horizontal pipe made of composite materials with a lumped mass, and the results showed that the lumped mass led to a decrease in critical flow velocity. Yamashita et al. (2022) examined the non-planar self-excited vibration in a vertically cantilevered pipe conveying fluid with an attached end mass. They found that both coupled plane and pendulum oscillations caused by nonlinear interactions between the third and fourth modes exhibited dynamic instabilities. Though various attempts have been made, previous research has only considered the inertial force of the lumped mass and has ignored the effects of gravity. This treatment is arguably suitable for horizontal and vertical pipes with high-frequency vibration because the gravity of the lumped mass has smaller effects than the inertial force in these cases. However, for the long pipes used in deep ocean mining and ocean thermal energy conversion, the internal flow-induced vibration has a relatively small frequency and amplitude. In these cases, the effects of gravity become important and ignoring the gravitational force leads to inaccurate or incorrect conclusions when the lumped mass effects are investigated. In addition, most previous studies only focused on lumped masses located at the free end of the pipes; few researchers have studied the effects of multiple lumped masses at arbitrary positions on the stability performance of vertical pipes.

In this regard, the present study intends to investigate the stability performance of a vertical cantilevered pipe conveying fluid with single and multiple lumped masses located at arbitrary positions. The governing vibration equation of the pipe with lumped masses is newly derived based on Hamilton's principle using delta and Heaviside functions. This new model is validated through comparison with published data. The harmonic differential quadrature (HDQ) method is applied to solve the vibration equation. Numerical simulations are performed to examine the effects of lumped mass weight, position, and fluid mass ratio. The numerical results show that lumped masses significantly affect the critical flow velocity, vibration frequency, and modal shapes. The lumped masses have both stabilizing and destabilizing effects on the pipe vibration induced by conveying internal flow. In order to reduce pipe vibration using lumped masses, careful investigation must be conducted with the number of lumped masses, weight, position, and fluid mass ratio all considered.

2. Governing vibration equations for pipe with multiple lumped masses

A sketch of a cantilevered pipe conveying fluid subjected to multiple lumped masses at various positions along the pipe is shown in Fig. 2. L is the total pipe length and x_{k} is the distance between the fixed end and the lumped mass position ($\mathrm{k} = 1, 2, \ldots$). U is the internal flow velocity, and D_o and D_i are the pipe's external and internal diameter, respectively. Multiple lumped masses m_{k} are attached to the pipe at the position x_{k}. The fluid in a vertical cantilevered pipe is conveyed through the fixed end to the free end. The pipe experiences vibration due to the transfer of energy from the internal flow to the pipe. Both inertial and gravitational forces act on the lumped mass during the pipe vibration.

The new vibration considering the pipe with lumped mass is derived by Hamilton's principle. The kinetic energy T of the system is the sum of the pipe kinetic energy T_1, fluid kinetic energy T_2, and lumped mass kinetic energy T_3.

$$T_1 = \frac{1}{2}\int_0^L m_p \left(\frac{\partial w}{\partial t}\right)^2 dx, \tag{1}$$

$$T_2 = \frac{1}{2}\int_0^L m_f \left\{U^2(\frac{\partial w}{\partial x})^2 + 2U\left(\frac{\partial^2 w}{\partial t \partial x}\right) + \left(\frac{\partial w}{\partial t}\right)^2\right\} dx, \tag{2}$$

$$T_3 = \frac{1}{2}\int_0^L \sum_{\mathrm{k}=1}^{\mathrm{K}} \left[m_{\mathrm{k}}\left(\frac{\partial w(x_{\mathrm{k}}, t)}{\partial t}\right)^2\right] dx, \tag{3}$$

where $w(x, t)$ is lateral displacement of the cantilevered pipe at position x at time t. m_f and m_p denote the mass of the fluid and pipe per unit length. K represents the total number of lumped masses on the pipe. $\delta(x - x_{\mathrm{k}})$ is a delta function, defined as $\delta() = 1$ for $x - x_{\mathrm{k}} = 0$ and $\delta() = 0$ for $x - x_{\mathrm{k}} \neq 0$.

The total potential energy V is the sum of the elastic potential energy of the pipe V_1, potential energy stored in the pipe and fluid V_2, and potential energy stored in the lumped mass V_3.

$$V_1 = \frac{1}{2}\int_0^L EI\left(\frac{\partial^2 w}{\partial x^2}\right)^2 dx, \tag{4}$$

$$V_2 = \frac{1}{2}\int_0^L (m_p + m_f)g(L - x)\left(\frac{\partial w}{\partial x}\right)^2 dx, \tag{5}$$

$$V_3 = \frac{1}{2}\int_0^L \sum_{\mathrm{k}=1}^{\mathrm{K}} \left[m_{\mathrm{k}} g H(x_{\mathrm{k}} - x)\left(\frac{\partial w(x_{\mathrm{k}}, t)}{\partial x}\right)^2\right] dx, \tag{6}$$

where EI is flexural rigidity, g is gravitational acceleration, and $H(x - x_{\mathrm{k}})$ is the Heaviside function, and is defined as $H() = 1$ for $x - x_{\mathrm{k}} \geq 0$ and $H() = 0$ for $x - x_{\mathrm{k}} < 0$.

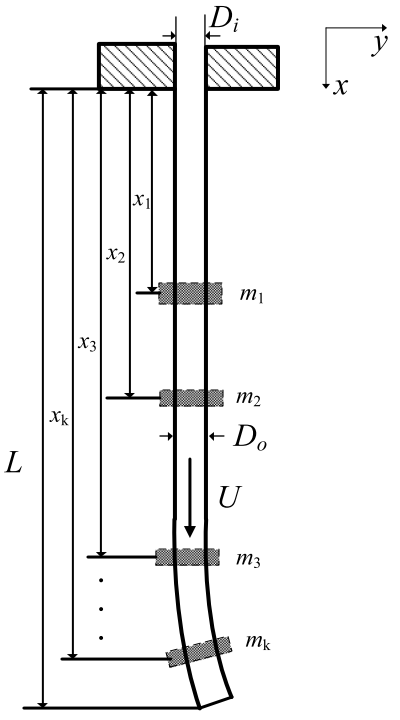

Fig. 2. Illustration of vertical cantilevered pipe conveying fluid with multiple lumped masses attached.

By applying Hamiltonian's principle, the motion of the dynamical system between two points with time interval t_1 to t_2 makes the line integral

$$\delta \int_{t_1}^{t_2} (T - V) dt = 0 \tag{7}$$

where T and V are the kinetic energy and potential energy, respectively, in the arbitrary time interval $[t_1 \quad t_2]$.

By substituting Eqs. (1)–(6) into Eq. (7), the new vibration equation is obtained. The details of this derivation are provided in Appendix A. The new vibration equation can be obtained as

$$\begin{aligned} &EI\frac{\partial^4 w}{\partial x^4} + [m_f U^2 - (m_p + m_f)g(L-x)]\frac{\partial^2 w}{\partial x^2} + 2m_f U\frac{\partial^2 w}{\partial x \partial t} + (m_p + m_f)\frac{\partial^2 w}{\partial t^2} \\ &+ (m_p + m_f)g\frac{\partial w}{\partial x} + \left[\sum_{k=1}^{K} m_k \delta(x - x_k)\right]\frac{\partial^2 w}{\partial t^2} - \left[\sum_{k=1}^{K} m_k g H(x_k - x)\right]\frac{\partial^2 w}{\partial x^2} = 0. \end{aligned} \tag{8}$$

Eq. (8) consists of seven terms:

1. $EI\frac{\partial^4 w}{\partial x^4}$, the flexural restoring force;
2. $m_f U^2 \frac{\partial^2 w}{\partial x^2}$, the internal flow-related centrifugal force;
3. $(m_p + m_f)g\frac{\partial w}{\partial x} - (m_p + m_f)g(L-x)\frac{\partial^2 w}{\partial x^2}$, the pipe and fluid gravity-induced tension;
4. $2m_f U\frac{\partial^2 w}{\partial x \partial t}$, the internal flow-related Coriolis force;
5. $(m_f + m_p)\frac{\partial^2 w}{\partial t^2}$, the inertial force of the fluid-filled pipe;
6. $\sum_{k=1}^{K} m_k \delta(x - x_k)\frac{\partial^2 w}{\partial t^2}$, the inertial force of the lumped mass;
7. $[\sum_{k=1}^{K} m_k g H(x_k - x)]\frac{\partial^2 w}{\partial x^2}$, the lumped mass gravity-induced tension.

Many researchers are concerned with the dynamic stability of pipes and have investigated the effects of lumped masses (Hill and Swanson, 1970; Wadham-Gagnon and Paidoussis, 2013; ElNajjar and Daneshmand, 2020; Khudayarov et al., 2020). However, they only considered the inertial force of the lumped mass and did not consider the effects of its gravity. In this study, both inertial and gravitational forces are considered in the vibration equation. The effects of the lumped mass can be accurately investigated to understand the critical flow velocity u_{cr}, frequency Ω_{cr}, and mode shapes.

The boundary conditions at the ends of the pipe are given as

$$\begin{aligned} &w(0,t)=0,\ \frac{\partial w(0,t)}{\partial x}=0, \quad at \quad x=0,\\ &\frac{\partial^2 w(L,t)}{\partial x^2}=0,\ \frac{\partial^3 w(L,t)}{\partial x^3}=0, \quad at \quad x=L. \end{aligned} \tag{9}$$

Eq. (8) can be rendered dimensionless through the use of the following dimensionless quantities as

$$\xi=\frac{x}{L},\ \zeta_{\mathrm{k}}=\frac{x_{\mathrm{k}}}{L},\ \eta=\frac{w}{L},\ \tau=\left(\frac{EI}{m_f+m_p}\right)^{1/2}\frac{t}{L^2}, \tag{10}$$

where ξ is a dimensionless axial spatial variable, ζ_{k} is the distance of the lumped mass from the fixed end, η is dimensionless lateral deflection, and τ is dimensionless time.

This yields the dimensionless equation of motion

$$\begin{aligned} &\frac{\partial^4\eta}{\partial\xi^4}+\left[u^2-\gamma(1-\xi)\right]\frac{\partial^2\eta}{\partial\xi^2}+\gamma\frac{\partial\eta}{\partial\xi}+2\beta^{1/2}u\frac{\partial^2\eta}{\partial\xi\partial\tau}+\frac{\partial^2\eta}{\partial\tau^2}\\ &+\left[\sum_{\mathrm{k}=1}^{\mathrm{K}}K_{\mathrm{k}}\delta(\xi-\zeta_{\mathrm{k}})\right]\frac{\partial^2\eta}{\partial\tau^2}-\left[\sum_{\mathrm{k}=1}^{\mathrm{K}}K_{\mathrm{k}}\gamma H(\zeta_{\mathrm{k}}-\xi)\right]\frac{\partial^2\eta}{\partial\xi^2}=0, \end{aligned} \tag{11}$$

with

$$\begin{aligned} &u=\left(\frac{m_f}{EI}\right)^{\frac{1}{2}}LU,\ \beta=\frac{m_f}{m_f+m_p},\ \gamma=\frac{(m_p+m_f)gL^3}{EI},\\ &K_{\mathrm{k}}=\frac{m_{\mathrm{k}}}{(m_f+m_p)L}. \end{aligned} \tag{12}$$

where u is dimensionless internal flow velocity. β and γ are the dimensionless fluid mass ratio and gravity parameter, respectively. K_{k} denotes the k-th dimensionless lumped mass ratio.

The corresponding boundary conditions are mathematically presented as

$$\begin{aligned} &\eta=0,\ \frac{\partial\eta}{\partial\xi}=0, \quad at \quad \xi=0,\\ &\frac{\partial^2\eta}{\partial\xi^2}=0,\ \frac{\partial^3\eta}{\partial\xi^3}=0, \quad at \quad \xi=1. \end{aligned} \tag{13}$$

3. Discretization of the pipe model

In this section, the HDQ method is introduced to discretize the equation of motion of the cantilevered pipe. The principle of the differential quadrature method is that any partial derivatives of a function at given grid points are approximated as the weighted linear sum of the function values at all grid points in the entire variable domain (Bert and Malik, 1996). Mathematically, application of the HDQ method to partial differential equations is expressed as

$$\frac{\partial^n f(x_{\mathrm{i}})}{\partial x^n}=\sum_{\mathrm{j}=1}^{N}A_{\mathrm{ij}}^{(n)}f(x_{\mathrm{i}}) \quad \mathrm{i,j}=1,2,\ldots,N, \tag{14}$$

where $f(x)$ is a continuous function, N denotes the total number of grid points in the domain, and the n-order denotes the partial derivatives of $f(x)$. $A_{\mathrm{ij}}^{(n)}$ are the weighting coefficients for n-order derivatives. Note that the weighting coefficients were derived by Ma et al. (2023) and are supplied in Appendix B.

For the vertical cantilevered pipe, the grid points are in the domain of ξ. Using the unequally spaced method to discretize ξ $(0\le\xi\le1)$, we obtain the grid point position with two adjacent μ-points ($\mu=10^{-6}\sim10^{-3}$) at the ends of the two boundaries. The unequally spaced sampling points with adjacent μ-points can be represented as

$$\begin{aligned} &\xi_1=0, \quad \xi_2=\mu,\\ &\xi_{\mathrm{i}}=\frac{1}{2}\left[1-\cos\left(\frac{\mathrm{i}-2}{N-3}\pi\right)\right] \quad (\mathrm{i}=3,4,\ldots,N-2),\\ &\xi_{N-1}=1-\mu, \quad \xi_N=1. \end{aligned} \tag{15}$$

Lateral deflection η still has the variables ξ and τ. The solution of Eq. (11) is represented as

$$\eta(\xi,\tau)=\Delta(\xi)e^{\Omega\tau}, \tag{16}$$

where Ω represents the eigenvalue of the pipe system. Δ is the displacement and is independent of time τ.

By substituting Eq. (16) into Eq. (11) and then applying the HDQ method to discretize the equations, the following discretization form is obtained:

$$\begin{aligned}&\sum_{j=1}^{N}\left\{A_{ij}^{(4)}+\left[u^2-\gamma(1-\xi)-\sum_{k=1}^{K}K_k\gamma H(\zeta_k-\xi)\right]A_{ij}^{(2)}+\gamma A_{ij}^{(1)}\right\}\Delta_j\\&+\Omega\left[\sum_{j=1}^{N}2\sqrt{\beta}uA_{ij}^{(1)}\right]\Delta_j+\Omega^2\left[1+\sum_{k=1}^{K}K_k\delta(\xi-\xi_k)\right]\Delta_i=0,\\&i=3,4,\ldots,N-2.\end{aligned}\tag{17}$$

Similarly, the boundary conditions are expressed as

$$\begin{aligned}&\Delta_1=0,\sum_{j=1}^{N}A_{1j}^{(1)}\Delta_j=0,\\&\sum_{j=1}^{N}A_{Nj}^{(2)}=0,\sum_{j=1}^{N}A_{Nj}^{(3)}\Delta_j=0.\end{aligned}\tag{18}$$

Eq. (17), combined with Eq. (18) yields the following set of linear equations:

$$\begin{bmatrix}1&0&0&0&0&\ldots&0\\A_{11}^{(1)}&A_{12}^{(1)}&A_{1(N-1)}^{(1)}&A_{1,N}^{(1)}&A_{1,3}^{(1)}&\ldots&A_{1(N-2)}^{(1)}\\A_{N1}^{(2)}&A_{N2}^{(2)}&A_{N(N-1)}^{(2)}&A_{NN}^{(2)}&A_{N3}^{(2)}&\ldots&A_{N(N-2)}^{(2)}\\A_{N1}^{(3)}&A_{N2}^{(3)}&A_{N(N-1)}^{(3)}&A_{NN}^{(3)}&A_{N3}^{(3)}&\ldots&A_{NN-2}^{(3)}\\H_{31}&H_{32}&H_{3(N-1)}&H_{3N}&H_{33}&\ldots&H_{3(N-2)}\\H_{41}&H_{42}&H_{4(N-1)}&H_{4N}&H_{43}&\ldots&H_{4(N-2)}\\\cdot&\cdot&\cdot&\cdot&\cdot&\ldots&\cdot\\\cdot&\cdot&\cdot&\cdot&\cdot&\ldots&\cdot\\\cdot&\cdot&\cdot&\cdot&\cdot&\ldots&\cdot\\H_{(N-2)1}&H_{(N-2)2}&H_{(N-2)(N-1)}&H_{(N-2)N}&H_{(N-2)3}&\ldots&H_{(N-2)(N-2)}\end{bmatrix}\begin{bmatrix}\Delta_1\\\Delta_2\\\Delta_{N-1}\\\Delta_N\\\Delta_3\\\Delta_4\\\cdot\\\cdot\\\cdot\\\Delta_{N-2}\end{bmatrix}$$
$$+\Omega\begin{bmatrix}0&0&0&0&0&\ldots&0\\0&0&0&0&0&\ldots&0\\0&0&0&0&0&\ldots&0\\0&0&0&0&0&\ldots&0\\S_{31}&S_{32}&S_{3(N-1)}&S_{3N}&S_{33}&\ldots&S_{3(N-2)}\\S_{41}&S_{42}&S_{4(N-1)}&S_{4N}&S_{43}&\ldots&S_{4(N-2)}\\\cdot&\cdot&\cdot&\cdot&\cdot&\ldots&\cdot\\\cdot&\cdot&\cdot&\cdot&\cdot&\ldots&\cdot\\\cdot&\cdot&\cdot&\cdot&\cdot&\ldots&\cdot\\S_{(N-2)1}&S_{(N-2)2}&S_{(N-2)(N-1)}&S_{(N-2)N}&S_{(N-2)3}&\ldots&S_{(N-2)(N-2)}\end{bmatrix}\begin{bmatrix}\Delta_1\\\Delta_2\\\Delta_{N-1}\\\Delta_N\\\Delta_3\\\Delta_4\\\cdot\\\cdot\\\cdot\\\Delta_{N-2}\end{bmatrix}\tag{19}$$
$$+\Omega^2\begin{bmatrix}0&0&0&0&0&\ldots&0\\0&0&0&0&0&\ldots&0\\0&0&0&0&0&\ldots&0\\0&0&0&0&0&\ldots&0\\0&0&0&0&1&\ldots&0\\0&0&0&0&0&\ldots&0\\\cdot&\cdot&\cdot&\cdot&\cdot&\ldots&\cdot\\\cdot&\cdot&\cdot&\cdot&\cdot&\ldots&\cdot\\\cdot&\cdot&\cdot&\cdot&\cdot&\ldots&\cdot\\0&0&0&0&0&\ldots&1\end{bmatrix}\begin{bmatrix}\Delta_1\\\Delta_2\\\Delta_{N-1}\\\Delta_N\\\Delta_3\\\Delta_4\\\cdot\\\cdot\\\cdot\\\Delta_{N-2}\end{bmatrix}=\begin{bmatrix}0\\0\\0\\0\\0\\0\\\cdot\\\cdot\\\cdot\\0\end{bmatrix}.$$

$\boldsymbol{H}_{ij}$ and $\boldsymbol{S}_{ij}$ denote the coefficient matrix of the Eq. (19) and are expressed explicitly as

$$\boldsymbol{H}_{ij}=A_{ij}^{(4)}+\left[u^2-\gamma+\gamma\xi_i-\sum_{k=1}^{K}K_k\gamma H(\zeta_k-\xi)\right]A_{ij}^{(2)}+\gamma A_{ij}^{(1)},\tag{20}$$

$$\boldsymbol{S}_{ij}=2\sqrt{\beta}uA_{ij}^{(1)},\tag{21}$$

where i = 3, 4, . . . , $N-2$, and j = 1, 2, . . . , N. When i = j, and the $\boldsymbol{S}_{\mathrm{ii}}$ is defined as

$$\boldsymbol{S}_{\mathrm{ii}} = 2\sqrt{\beta}uA_{\mathrm{ii}}^{(1)}. \tag{22}$$

Eq. (19) can be written as

$$\begin{aligned}
&\begin{bmatrix} \boldsymbol{A}_{bb} & \boldsymbol{A}_{bd} \\ \boldsymbol{A}_{db} & \boldsymbol{A}_{dd} \end{bmatrix}\begin{Bmatrix} \boldsymbol{\Delta}_b \\ \boldsymbol{\Delta}_d \end{Bmatrix} + \Omega\begin{bmatrix} \boldsymbol{0} & \boldsymbol{0} \\ \boldsymbol{B}_{db} & \boldsymbol{B}_{dd} \end{bmatrix}\begin{Bmatrix} \boldsymbol{\Delta}_b \\ \boldsymbol{\Delta}_d \end{Bmatrix} \\
&+ \Omega^2\begin{bmatrix} \boldsymbol{0} & \boldsymbol{0} \\ \boldsymbol{0} & \boldsymbol{I} \end{bmatrix}\begin{Bmatrix} \boldsymbol{\Delta}_b \\ \boldsymbol{\Delta}_d \end{Bmatrix} = \begin{Bmatrix} \boldsymbol{0} \\ \boldsymbol{0} \end{Bmatrix}, \\
&\boldsymbol{\Delta}_b = (\Delta_1 \quad \Delta_2 \quad \Delta_{N-1} \quad \Delta_N), \\
&\boldsymbol{\Delta}_d = (\Delta_3 \quad \Delta_4 \quad \ldots \quad \Delta_{N-2}),
\end{aligned} \tag{23}$$

where the subscript b indicates an element closely related to the boundary points, and d is another element. $\boldsymbol{0}$ denotes the null matrix, $\boldsymbol{I}$ represents the identity matrix with order $d \times d$, and $\boldsymbol{\Delta} = (\boldsymbol{\Delta}_b \quad \boldsymbol{\Delta}_d)^T$.

By eliminating $\boldsymbol{\Delta}_b$, the following homogeneous equation can be derived:

$$[\Omega^2\boldsymbol{M} + \Omega\boldsymbol{C} + \boldsymbol{K}]\boldsymbol{\Delta}_d = \boldsymbol{0}, \tag{24}$$

where $\boldsymbol{M}$, $\boldsymbol{C}$ and $\boldsymbol{K}$ denote the structural mass matrix, damping matrix, and stiffness matrix, respectively. The matrices $\boldsymbol{C}$ and $\boldsymbol{K}$ are calculated as

$$\boldsymbol{C} = -\boldsymbol{B}_{db}\boldsymbol{A}_{bb}^{-1}\boldsymbol{A}_{bd} + \boldsymbol{B}_{dd}, \quad \boldsymbol{K} = -\boldsymbol{A}_{db}\boldsymbol{A}_{bb}^{-1}\boldsymbol{A}_{bd} + \boldsymbol{A}_{dd}. \tag{25}$$

The solution of Eq. (24) is transformed into the eigenvalues of the following matrix:

$$\boldsymbol{E} = \begin{bmatrix} \boldsymbol{0} & \boldsymbol{I} \\ -\boldsymbol{M}^{-1}\boldsymbol{K} & -\boldsymbol{M}^{-1}\boldsymbol{C} \end{bmatrix}. \tag{26}$$

By solving the matrix E, the eigenvalue Ω can be obtained, which is a series of complex numbers Ω=Re(Ω)+iIm (Ω), where i is the imaginary unit. The real part of Ω, Re(Ω), corresponds to the dimensionless frequency of vibration, and the imaginary part, Im (Ω), is related to damping. A negative value of the imaginary part of the dimensionless eigenvalues indicates that the pipe is unstable, leading to pipe flutter or static divergence. Whenever Im(Ω) = 0 and Re(Ω) ≠ 0, this signifies pipe amplified oscillation known as flutter; conversely, if Re(Ω) = 0, then a static instability occurs, identified as static divergence.

4. Results and discussion

4.1. Theoretical model validation

A numerical investigation was conducted to validate the theoretical model and compare it with those of ElNajjar and Daneshmand (2020) and Yi et al. (2020). Numerical simulations were performed for a pipe conveying fluid with $\gamma = 10$, $K_1 = 0.2$, and $\zeta_1 = 0.5$. The dimensionless critical flow velocity u_{cr} for various dimensionless mass ratios β are shown in Fig. 3. The present results are in excellent agreement with ElNajjar and Daneshmand (2020). It should be emphasized that both models ignored the gravitational force in these simulations. The proposed theoretical model is further compared with the experimental results of Yi et al. (2020) to demonstrate the importance of lumped masses and the corresponding gravitational force. No lumped masses were included, and only inertial force-including cases are presented. Table 1 shows that the lumped mass has noticeable effects on the pipe's critical flow velocity and that the proposed model produces better results than the previous model when compared with the experimental data. Differences of less than 3% occurs for various cases. From a physical point of view, when the lumped mass is installed on the vertical cantilevered pipe, the pipe is subject to the gravity of the lumped mass and produces a vertical tension force. When the pipe vibrates under the internal flow, it is subject to the inertial and tension forces of the lumped mass simultaneously. Only when gravity and the inertial force of the lumped mass are considered simultaneously can the vibration characteristics of the pipe be accurately reflected. A large error can occur if only the inertial force of the weight is considered.

4.2. Single lumped mass effects

4.2.1. Single lumped mass weight effect

Five different weights, that is, no lumped mass, $K_1 = 0.1$, 0.2, 0.5, and 1, were considered. Fig. 4 represents the critical flow velocity u_{cr} and frequency Ω_{cr} for a cantilevered pipe with various lumped masses K_1. The first case, represented by the black square (■), is the original cantilevered pipe with no lumped mass. The S-shaped curves illustrate the vertical cantilevered pipe with no lumped mass and exhibit trends similar in all cases. It is shown in Fig. 4(a) that increasing the lumped mass decreases the critical flow velocity values, i.e. a lumped mass on a vertical cantilevered pipe at the free end has a destabilizing effect. The critical flow velocity of the pipe increases as β increases regardless of the value of K_1. A clear

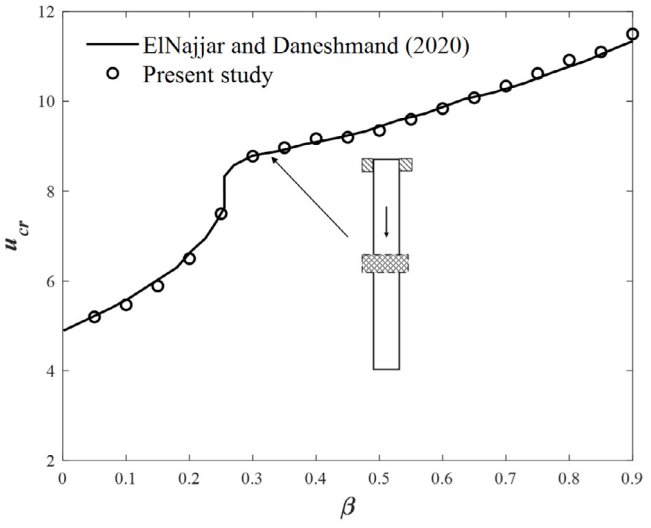

Fig. 3. The effects of a lumped mass on the critical flow velocity u_{cr} as a function of the parameter β for different lumped mass values for $\gamma = 10$, $K_1 = 0.2$ and $\zeta_1 = 0.5$.

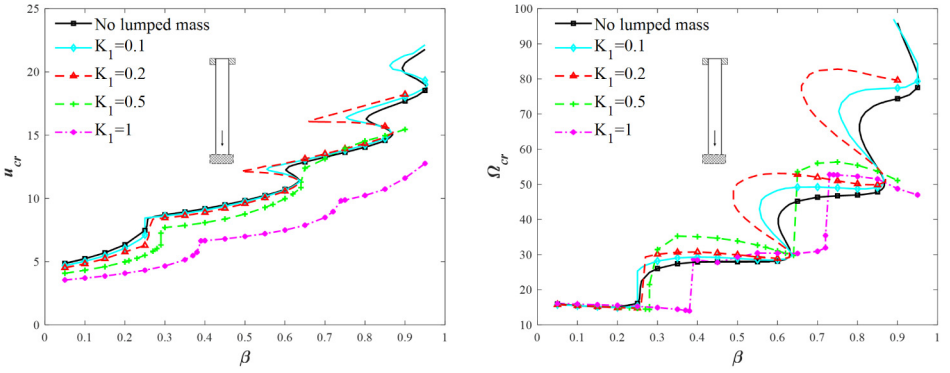

Fig. 4. The effect of a lumped mass on the critical flow velocity u_{cr} and frequency Ω_{cr} as a function of the parameter β for different lumped mass values for $\gamma = 10$ and $\zeta_1 = 1$.

Table 1
Comparison between the present study and Yi et al. (2020) experimental results for $\beta = 0.313$, $\gamma = 51.69$ and $K_1 = 0.437$.

	$\zeta_1 = 0.5$	$\zeta_1 = 0.82$	$\zeta_1 = 0.95$
No lumped mass included	$u_{cr} = 10.12$	$u_{cr} = 10.12$	$u_{cr} = 10.12$
Only inertial force included	$u_{cr} = 10.14$	$u_{cr} = 8.99$	$u_{cr} = 7.98$
Both inertial force and gravity included	$u_{cr} = 10.54$	$u_{cr} = 9.47$	$u_{cr} = 8.4$
Yi et al. (2020)	$u_{cr} = 10.78$	$u_{cr} = 9.64$	$u_{cr} = 8.48$
Difference (%)	2.2	1.7	0.9

"jump" is observed in the critical frequency for $K_1 = 0.5$ and 1, as shown in Fig. 4(b). This is mainly because when the weight of the lumped mass increases, the lower-mode unstable balance state undergoes a transient change and reaches a new state of equilibrium, leading to the mode jumping, which triggers the occurrence of the "jump" phenomenon.

Fig. 5 shows the first modal shapes of the cantilevered pipe conveying fluid with various K_1 values for $\beta = 0.3$. The maximum displacement of the pipe occurs at the free end when no lumped mass is included ($K_1 = 0$). However, with a lumped mass, $K_1 > 0$, the maximum amplitude of the first modal shape occurs at a position above the free end. It was observed that as K_1 increased, the displacement decreased. However, the maximum displacement first decreased and then increased. When the lumped mass is installed at the free end of the pipe, the pipe is under gravity-induced tension. When pipe vibration occurs, the free end of the pipe is affected by the tensioning force of the lumped mass, resulting in the maximum amplitude of the pipe occurring above the free end. In addition, the heavier the lumped mass, the smaller the

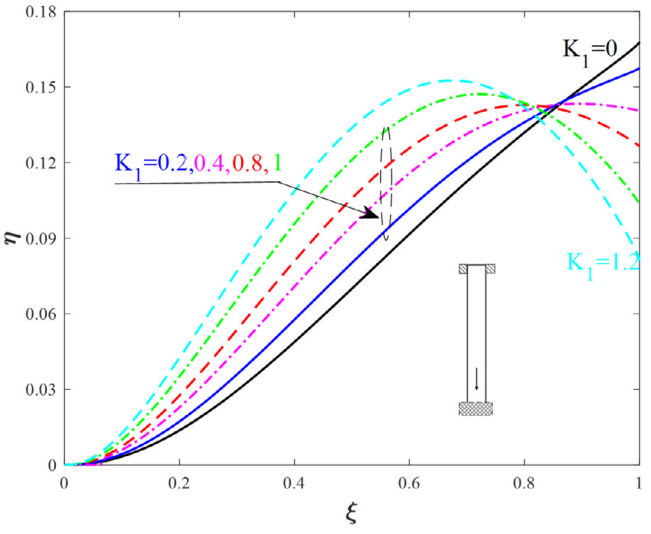

Fig. 5. The first mode shape of the pipe with different lumped mass weights for $u = 3$ for $\beta = 0.3$.

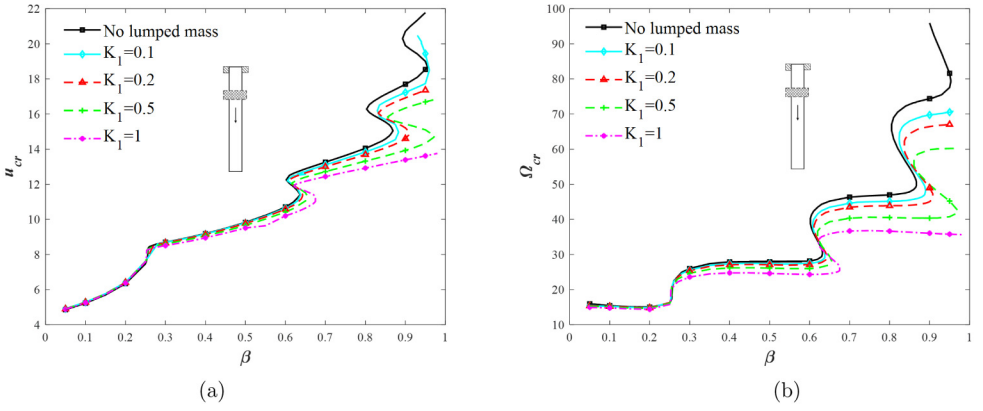

Fig. 6. The effect of a lumped mass on the critical flow velocity u_{cr} and frequency Ω_{cr} as a function of the parameter β, with different lumped mass values for $\gamma = 10$ and $\zeta_1 = 0.25$.

amplitude of the pipe; therefore, a reasonable choice of the weight of the lumped mass has a significant influence on the stability of the pipe.

Different lumped mass weights were investigated at various positions in the pipe. Each case consisted of five different lumped mass ratios K_1 at the position ζ_1. The results for the first three cases are shown in Figs. 6–8, respectively. From the first case ($\zeta_1 = 0.25$, $K_1 = 0.1$, $K_1 = 0.2$, $K_1 = 0.5$, $K_1 = 1$), it can be concluded that the lumped mass beside the clamped end has a marginal effect on the pipe for $0.05 < \beta < 0.25$, as shown in Fig. 6. It should be noted that any lumped mass in a pipe with $\beta > 0.25$ has a destabilizing effect. The critical frequency of the pipe decreases as the lumped mass increases. For $\zeta_1 = 0.25$, the lumped mass has a marginal effect on the pipe for $0.05 < \beta < 0.25$, as shown in Fig. 6. Note that any lumped mass for $\beta > 0.25$ has a destabilizing effect. The critical frequency of the pipe decreases as the lumped mass increases, regardless of the value of β.

A lumped mass can increase stability when it is positioned in the middle ($\zeta_1 = 0.5$) for $\beta < 0.4$ and reduce the stability for $\beta > 0.4$, as shown in Fig. 7. The S-shaped curve for $K_1 = 0$ gradually disappears as K_1 increases. Moreover, the critical flow frequency of the pipe decreases as the lumped mass increases. For $\zeta_1 = 0.75$, as shown in Fig. 8, the lumped mass has a strong destabilizing effect, regardless of the weight.

4.2.2. Single lumped mass position effect

Argand diagrams depicting the pipe vibration characteristics of lumped masses located at different positions are shown in Fig. 9(a)–(d). These figures show the first four modes of the pipe with $\beta = 0.3$, $\gamma = 10$, and $K_c = 0.5$.

The critical flow velocity is 8.7 in the second mode (Fig. 4) when no lumped mass is included. The critical flow velocity is reduced to $u = 8.59$, which corresponds to the flutter instability in the third mode for $\zeta_1 = 0.25$. This indicates that the

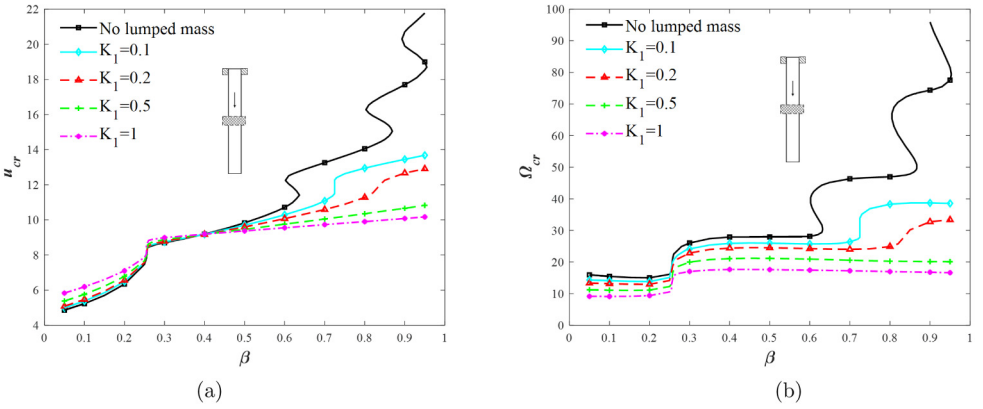

Fig. 7. The effect of a lumped mass on the critical flow velocity u_{cr} and frequency Ω_{cr} as a function of the parameter β for different lumped mass values for $\gamma = 10$ and $\zeta_1 = 0.5$.

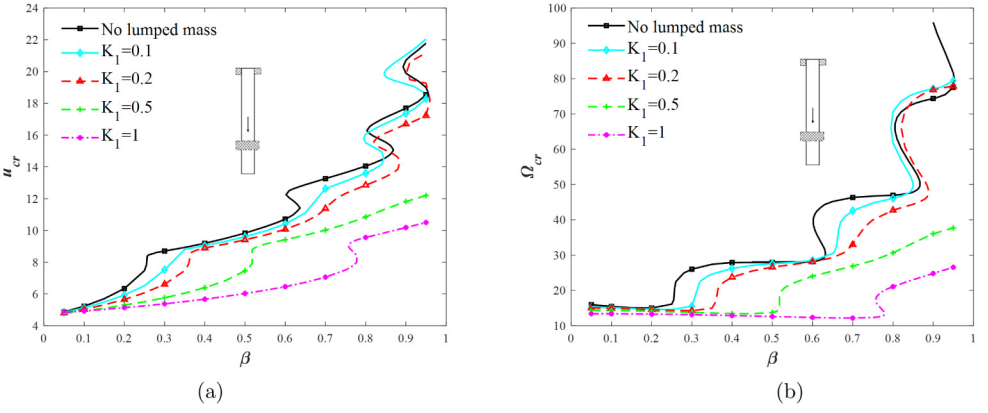

Fig. 8. The effect of a lumped mass on the critical flow velocity u_{cr} and frequency Ω_{cr} as a function of the parameter β for different lumped mass values for $\gamma = 10$ and $\zeta_1 = 0.75$.

introduction of a lumped mass can decrease the critical flow velocity and thus reduce the stability of the cantilevered pipe. It is noteworthy that the critical flow velocity increases to 8.8 and corresponds to flutter instability in the second mode when the lumped mass is located at $\zeta_1 = 0.5$. For $\zeta_1 = 0.75$, the critical flow velocity decreases to 5.7, corresponding to the flutter instability in the second mode. When the lumped mass is positioned at $\zeta_1 = 1$, the critical flow velocity increases to 7.7 and the corresponding instability mode shifts to the third mode. We conclude that the critical flow velocity shows a complex trend when the position of the lumped mass changes from the fixed end to the free end. This is primarily because the lumped mass generates inertia force and gravity on the pipe (Eq. (8) terms 6–7), and its two parameters can change the stiffness and mass matrices of the system (Eq. (19) terms 1 and 2). When the lumped mass is closer to the free end of the pipe, the influence on the parameters of the stiffness matrix is greater, such that the unstable equilibrium state of the mode changes instantaneously and reaches a new equilibrium state, which leads to mode jumping. Therefore, the critical flow velocity and frequency experience "jumps".

The effect of the lumped mass position was investigated further by considering two cases. Each case consisted of four different positions with a lumped mass ratio K_1 at position ζ_1. These two cases are illustrated in Figs. 10–11, respectively. In the first cases ($\zeta_1 = 0.25$, $\zeta_1 = 0.5$, $\zeta_1 = 0.75$, $K_1 = 0.2$), when the lumped mass was located near the top end, little effect was observed on the pipe. The stability marginally changed when the lumped mass was at the mid-pipe ($\zeta_1 = 0.5$) for $0.05 < \beta < 0.4$, whereas the lumped mass destabilized the pipe for higher values of β. For a larger lumped mass $K_1 = 0.5$, the lumped mass generally reduced the pipe stability, except in the case where $\zeta_1 = 0.5$ and $0.05 < \beta < 0.4$, as shown in Fig. 11.

Fig. 12 illustrates the influence of a lumped mass at various positions on (a) the critical flow velocity u_{cr} and (b) critical frequency Ω_{cr} for $\beta = 0.3$ and $\gamma = 10$. When the lumped mass position ζ_1 is less than 0.33, the critical flow velocity remains approximately constant and then increases when $0.33 < \zeta_1 < 0.44$. The critical flow velocity decreases and then increases as ζ_1 increases. When the lumped mass is located above $\zeta_1 = 0.33$, the critical frequency remains approximately constant as ζ_1 increases. When ζ_1 increases from 0.33 to 0.6, the critical frequency begins to gradually

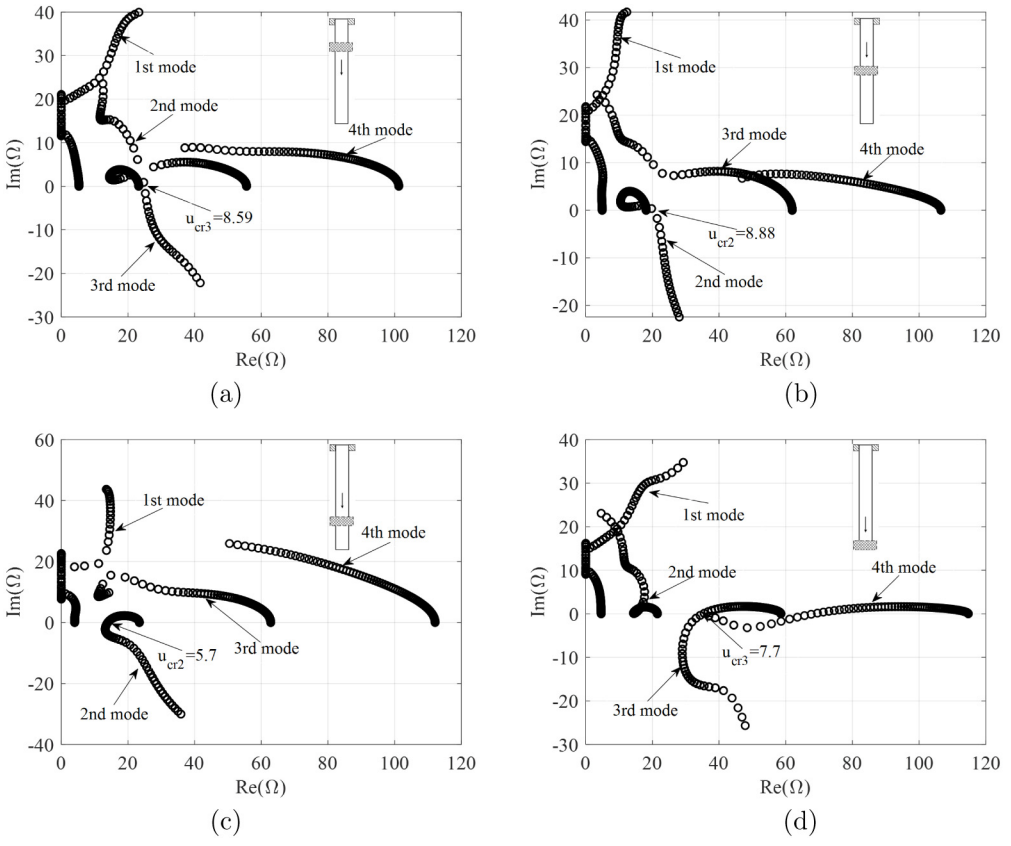

Fig. 9. Dimensionless complex frequency of the first four modes as the flow velocity u for different positions of the lumped mass with $\beta = 0.3$, $\gamma = 10$ and $K_1 = 0.5$: (a) $\zeta_1 = 0.25$; (b) $\zeta_1 = 0.5$; (c) $\zeta_1 = 0.75$; (d) $\zeta_1 = 1$.

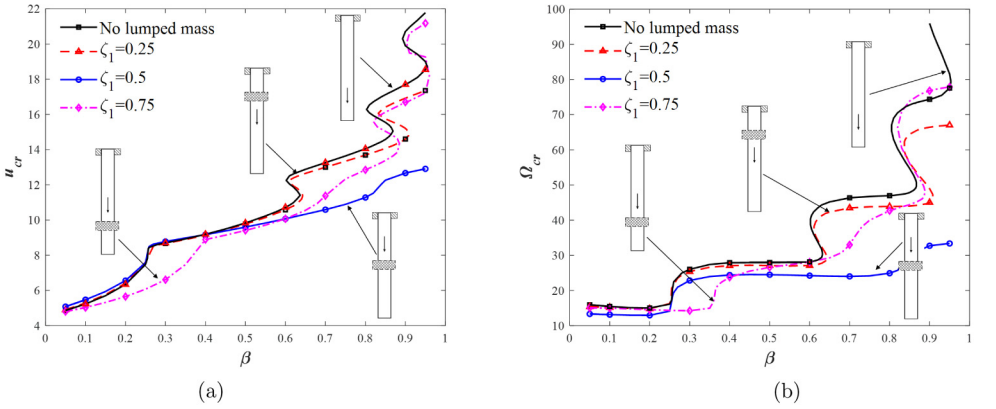

Fig. 10. The effect of a lumped mass on the critical flow velocity u_{cr} and frequency Ω_{cr} as a function of the parameter β for different lumped mass positions with $\gamma = 10$ and $K_1 = 0.2$.

decrease and reaches the lowest point at approximately $\zeta_1 = 0.6$. Then, the critical frequency gradually increases when $\beta > 0.6$.

Consider a cantilevered pipe with a lumped mass at the quarter position of the pipe (for example, the curve in Fig. 7 with $\zeta_1 = 0.25$, $K_1 = 0.5$). These curves have "S-shaped" portions ((Hill and Swanson, 1970) called "knees") in the critical flow velocity and frequency curves in the ranges $0.615 < \beta < 0.655$ and $0.855 < \beta < 0.97$. The Argand diagram of a cantilevered pipe with one lumped mass ($\zeta_1 = 0.25$, $K_1 = 0.5$) with $\beta = 0.63$ are shown in Fig. 13. As shown, as internal flow velocity u increases, the imaginary part of the first mode frequency moves into the lower half-plane, moves back to the upper half-plane, and finally moves back into the lower half-plane and stays there. It should be noted that the

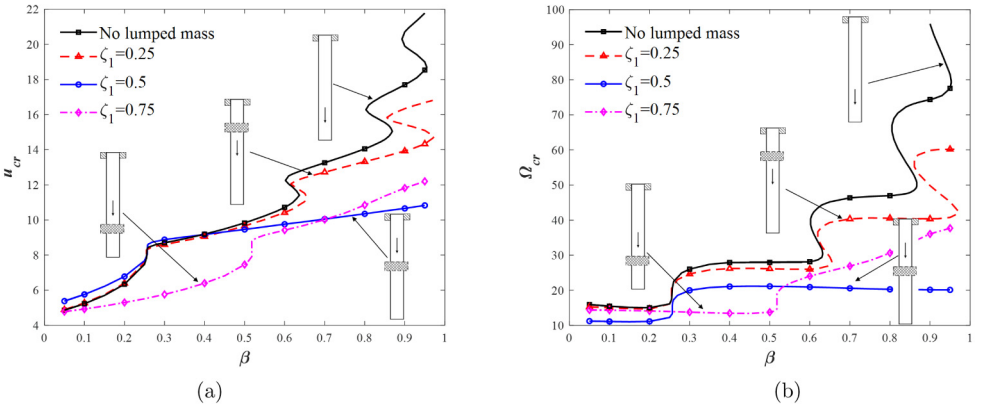

Fig. 11. The effect of a lumped mass on the critical velocity u_{cr} and frequency Ω_{cr} as a function of the parameter β for different lumped mass positions with $\gamma = 10$ and $K_1 = 0.5$.

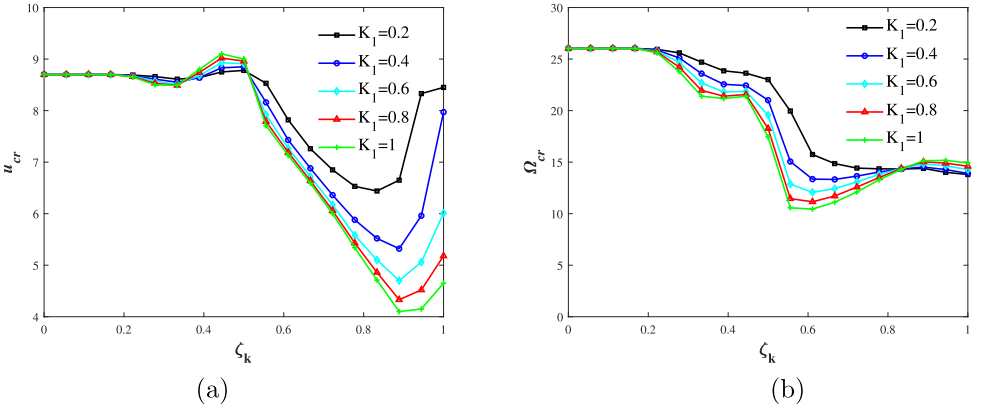

Fig. 12. The critical flow velocity of the instability of the pipe varying with the lumped mass position at different lumped mass ratio for $\beta = 0.3$.

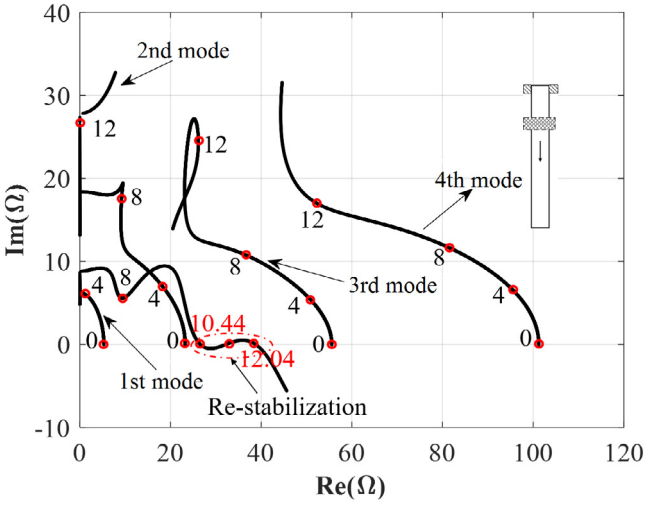

Fig. 13. Argand diagrams of a cantilevered pipe with one lumped mass ($\zeta_1 = 0.25$, $K_1 = 0.5$) with $\beta = 0.63$.

cantilevered pipe restabilizes at $\beta = 0.63$, corresponding to three critical flow velocity values. This knee-type behavior was also reported in Paidoussis (1970) and Hill and Swanson (1970).

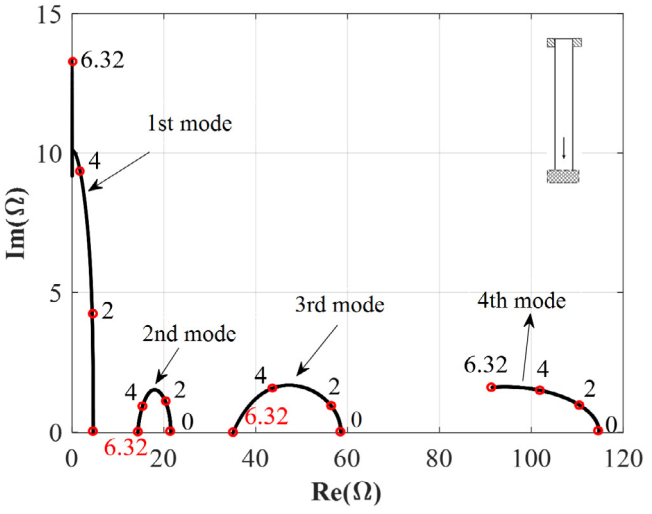

Fig. 14. Argand diagrams of a cantilevered pipe with one lumped mass ($\zeta_1 = 1$, $K_1 = 0.5$) with $\beta = 0.29$.

Consider a cantilevered pipe with a lumped mass at the free end (for example, the curve in Fig. 4 with $\zeta_1 = 1, K_1 = 0.5$), there are 'kinks' in the critical flow velocity curve and 'jumps' in the critical frequency curve for $\beta = 0.29$. The Argand diagram of a cantilevered pipe having one lumped mass ($\zeta_1 = 1$, $K_1 = 0.5$) with $\beta = 0.29$, as shown in Fig. 14. It is observed that, as internal flow velocity u approaches u_{cr} for $\beta = 0.29$, the characteristic roots of 2nd and 3rd modes approach the imaginary axis at the same value of u: $u_{cr} = 6.32$. The characteristic root of 2nd mode crosses the imaginary axis before the characteristic root of 3rd mode for $\beta < 0.29$. Furthermore, the characteristic root of 3rd mode moves the imaginary axis before the characteristic root of 2nd mode in $\beta > 0.29$.

Fig. 15 displays the variation of vibration frequency mode jumps with the location of the lumped mass, where n denotes the mode number. For $\beta = 0.1$, there is no mode change as the location of the lumped mass changes, whereas for $\beta = 0.3$, the critical frequency is mainly concentrated in the second mode, and the mode jumps to the third mode at $0.28 < \zeta_1 < 0.5$ and $0.94 < \zeta_1 < 1$. For $\beta = 0.5$, the critical frequency is mainly concentrated in the third mode, and the mode jumps to the second mode at $0.38 < \zeta_1 < 0.83$. For $\beta = 0.7$, the vibration mode gradually jumps from the first to the fourth mode.

The pipe vibration mode jumping refers to the phenomenon when solving the eigenvalues of the system vibration characteristic equation in which a small change in the structural stiffness and mass matrix can cause a sharp change in some of the structural modal data, resulting in a jump. When the lumped mass is located on the pipe, the inertia $\sum_{k=1}^{K} m_k \delta(x - x_k) \frac{\partial^2 w}{\partial t^2}$ and gravity $[\sum_{k=1}^{K} m_k g H(x_k - x)] \frac{\partial^2 w}{\partial x^2}$ terms of the lumped mass are added to the control equation, and after discretizing the equation of motion, these two parameters change the mass and stiffness matrices of the system. As the location of the lumped mass changes, the mass and stiffness matrix data of the system change dramatically, such that the ordering of the eigenvalues of each mode changes when solving for the eigenvalues, resulting in changes in the vibration modes.

Fig. 16 shows the effect of lumped mass position on the model shape for $\beta = 0.3$, $K_1 = 0.8$ and $u = 3$. The maximum amplitude of the pipe does not always occur at the end of the pipe, but may appear at some position in the upper part of the pipe. The vibration amplitude of the pipe increases and then decreases when the lumped mass position ζ_1 increases from 0 to 1. The maximum amplitude η_{max} of the pipe at $\zeta_1 = 0.75$ was 0.192, whereas the minimum amplitude was 0.143 at $\zeta_1 = 1$. It was observed that the amplitude of the pipe can be effectively reduced when the lumped mass is installed at the free end.

According to the results in Table 2, the vibration amplitude increases with an increase in ζ_1 when the lumped mass is installed in the range of 0 to 0.75. When the lumped mass is located closer to the free end of the pipe ($\zeta_1 > 0.75$), the vibration mode of the pipe transitions from second-to third mode shape (as shown in Fig. 9) and the amplitude decreases. Taking the case of $K_1 = 0.6$ as an example, by moving the lumped mass position ζ_1 from 0 to 0.75, the pipe vibration amplitude increases from 0.167 to 0.201, which is a 20.3% increase. However, when the lumped mass position ζ_1 moves from 0.75 to 1, the pipe vibration amplitude decreases from 0.201 to 0.142, that is, it decreases by 29.3%. This is mainly a result of the transition of vibration modes when the lumped mass is installed at different positions in the pipe.

4.3. Multiple lumped mass effects

The effects of multiple lumped masses were studied by considering five different lumped mass positions, as shown in Fig. 17. Each case has two lumped masses $K_1 = K_2 = 0.5$ at position ζ_k (k = 1, 2). The stabilization effects are evident

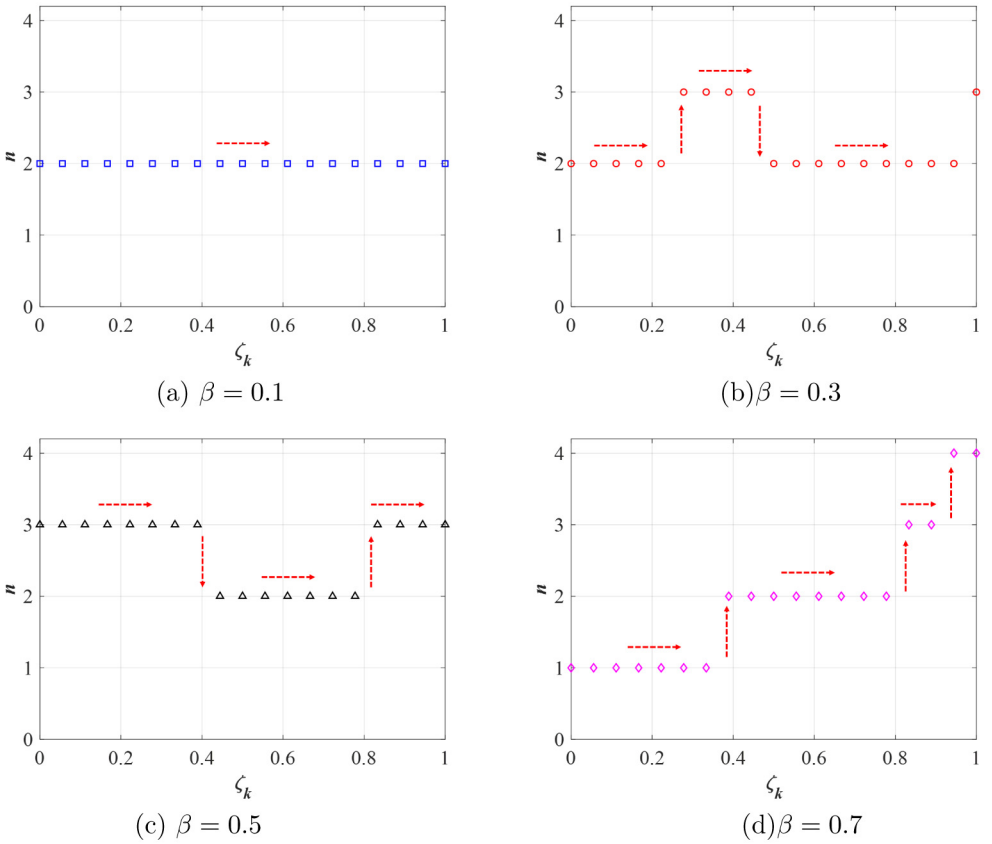

Fig. 15. Variation of mode jumps with the location of the lumped mass (n is the mode number): (a) $\beta = 0.1$; (b) $\beta = 0.3$; (c) $\beta = 0.5$; (d) $\beta = 0.7$.

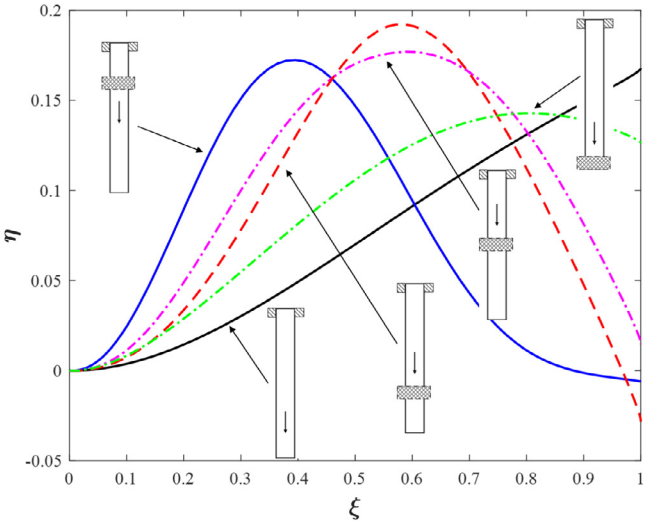

Fig. 16. The modal shape of a pipe conveying fluid varying with the lumped mass position for $\beta = 0.3$, $\gamma = 10$ and $u = 3$.

when the lumped mass is in the upper part of the pipe length ($\zeta_1 = 0.25$, $\zeta_2 = 0.5$) for $0.05 < \beta < 0.65$. When the pipe is attached to the two lumped masses, the different positions of the lumped mass affect the magnitude of the critical flow velocity of the cantilevered pipe. Taking $\beta = 0.3$ as an example, the critical flow velocity of the pipe is 71.8% higher when the two lumped masses are located at $\zeta_1 = 0.25$ and $\zeta_2 = 0.5$ than when $\zeta_1 = 0.75$ and $\zeta_2 = 1$. In Fig. 18, three

Table 2
Maximum vibration amplitude η_{max} of the cantilevered pipe conveying fluid at different lumped mass positions for $\beta = 0.3$ and $\gamma = 10$..

ζ_1	$K_1 = 0.2$	$K_1 = 0.4$	$K_1 = 0.6$	$K_1 = 0.8$	$K_1 = 1$
0	0.167	0.167	0.167	0.167	0.167
0.25	0.179	0.176	0.174	0.171	0.169
0.5	0.188	0.185	0.182	0.177	0.172
0.75	0.265	0.257	0.201	0.192	0.183
1	0.149	0.143	0.142	0.143	0.147

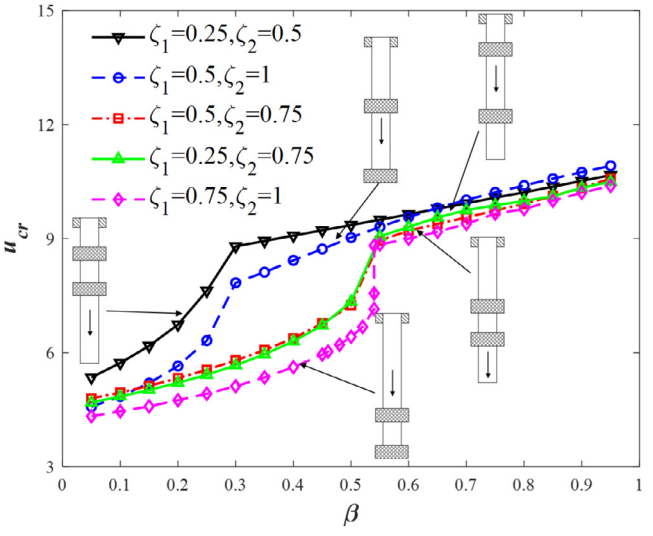

Fig. 17. The effects of two lumped masses on the critical flow velocity u_{cr} as a function of the parameter β for different lumped mass positions with $\gamma = 10$ and $K_1 = K_2 = 0.5$.

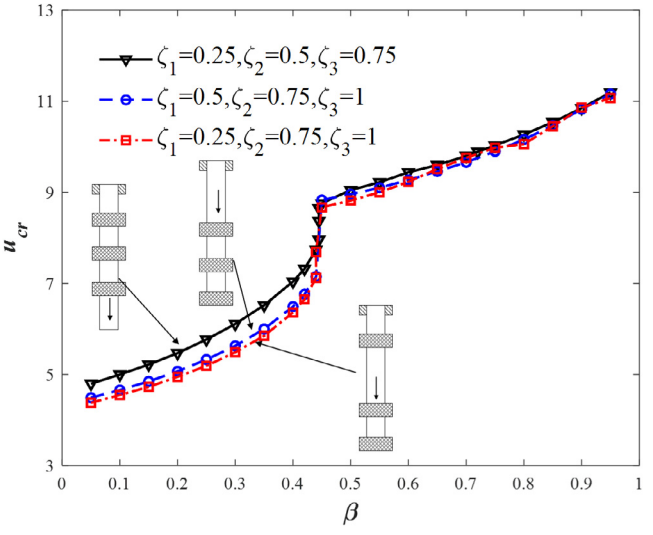

Fig. 18. The effects of three lumped masses on the critical flow velocity u_{cr} as a function of the parameter β for different lumped mass positions with $\gamma = 10$ and $K_1 = K_2 = K_3 = 1/3$.

cases are considered to study the effects of three lumped masses at different positions of the pipe. It was observed that multiple lumped masses have limited effects on the critical flow velocity.

The effects of multiple lumped masses on the critical flow velocity u_{cr} were investigated further. In each case, the total dimensionless weight of the lumped mass is $\sum_{k=1}^{K} K_k = 1$. The shaped curve of the position at the top represents the vertical cantilevered pipe without a lumped mass in Fig. 19. The lumped mass effects depend on the number of lumped

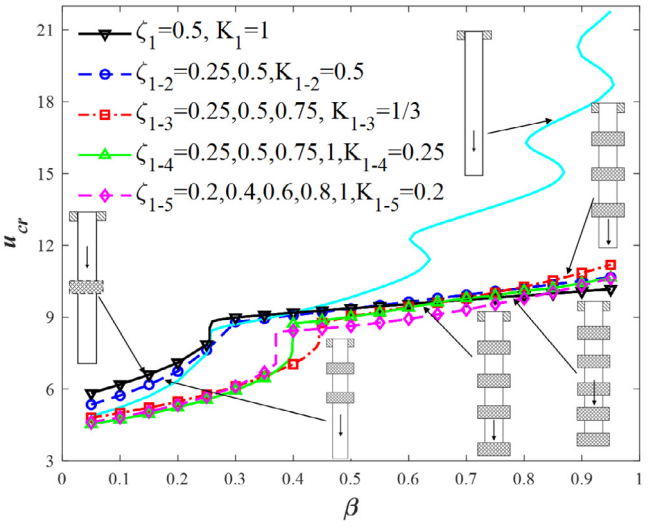

Fig. 19. The effects of multiple lumped masses on the critical flow velocity u_{cr} as a function of the parameter β for different lumped mass positions with $\gamma = 10$.

masses and the mass-fluid ratios β. It can be observed that the critical flow velocity of the cantilevered pipe increases as β increases regardless of the number of lumped masses. The lumped mass stabilizes the cantilevered pipe when it is positioned in the middle ($\zeta_1 = 0.5$) for $\beta < 0.4$, and destabilizes the pipe for $\beta > 0.4$. Similarly, the two lumped masses stabilize the cantilevered pipe when the lumped masses are positioned in the middle ($\zeta_1 = 0.25$, $\zeta_2 = 0.5$) for $\beta < 0.25$, whereas they destabilize the pipe for $\beta > 0.25$. It is noteworthy that the vertical cantilevered pipe becomes more destabilized when three or more lumped masses are attached to it. Moreover, when three or more lumped masses are attached to the vertical cantilever pipe, the curves almost overlap at $\beta < 0.35$, indicating that the lumped mass effects are ignored in these cases. When the number of lumped masses on the pipe increases, the result is equivalent to increasing the mass per unit length, which results in a decrease in the fluid mass ratio $\beta = m_f/(m_f + m_p)$, thus causing a decrease in the critical flow velocity of the pipe.

Contrary to the conventional understanding, installing lumped masses on a pipe does not always improve the pipe stability; the results are highly dependent on the position and number of lumped masses installed. In particular, during actual field operation, the position and weight of the lumped mass must be reasonably designed to minimize the vibration of deep-sea mining discharging pipes. The proper design of lumped masses can improve pipe stability. However, an improper design reduces pipe stability. The numerical results of this study can provide theoretical support for the reasonable arrangement of submersible pumps for deep-sea mining discharging pipes.

5. Conclusion

In this study, the stability of a vertical cantilevered pipe conveying fluid with single and multiple lumped masses was analyzed. The HDQ method was utilized to solve the governing vibration equation, which was derived based on Hamilton's principle and the introduction of the delta and Heaviside functions. The gravitational force of the lumped mass is considered in the theoretical model. The newly developed model was validated by comparison with previously published data. The pipe's instability performance was analyzed using this new model for various lumped mass weights, positions, and fluid mass ratios. From the numerical results, the following conclusions were drawn.

(1) Increasing the lumped mass improves stability when the lumped mass is positioned in the middle ($\zeta_1 = 0.5$) for $\beta < 0.4$ and decreases stability for $\beta > 0.4$. However, the critical flow velocity decreases for all values of β for pipes with more than two lumped masses.

(2) The lumped mass significantly affects the modal shape of the vertical cantilevered pipe. Larger lumped mass ratios do not guarantee that the maximum amplitude of the modal ratio always occurs at the end of the pipe; it may occur higher up. Increasing the lumped mass ratios can decrease the modal shape amplitude. The pipe amplitude reaches a minimum when the lumped mass is attached to the free end of the pipe, whereas the amplitude is at its maximum at three-quarters of the pipe.

(3) When the lumped mass position ζ_1 increases from 0 to 1, the critical vibration mode of the cantilevered pipe shifts. When the fluid mass ratio is sufficiently large, the vibration mode of the cantilevered pipe also shifts.

(4) The lumped mass position and fluid mass ratio are important factors affecting the stability of cantilevered pipes. The critical velocity of the cantilevered pipe varies with the lumped mass position and fluid mass ratio.

(5) Regardless of the weight of the lumped mass, the lumped mass at a position close to the clamping end did not significantly affect the dynamic behavior of the cantilevered pipe length.

(6) The vertical cantilevered pipe is destabilized when two or more lumped masses are present as compared to the case of a single lumped mass.

These conclusions are expected to provide valuable guidance for engineering applications, such as deep-sea mining and OTEC, with the purpose of alleviating pipe vibrations using the lumped mass method.

CRediT authorship contribution statement

Yongqi Ma: Conceptualization, Methodology, Software, Validation, Formal analysis, Data curation, Investigation, Writing – original draft. **Dingchang Zhou:** Formal analysis, Data curation, Investigation. **Yunxiang You:** Funding acquisition, Project administration, Supervision. **Yijun Shen:** Visualization, Investigation. **Ke Chen:** Conceptualization, Writing – review & editing. **Aichun Feng:** Conceptualization, Writing – review & editing, Funding acquisition, Project administration, Supervision.

Declaration of competing interest

The authors declare that they have no known competing financial interests or personal relationships that could have appeared to influence the work reported in this paper.

Data availability

Data will be made available on request.

Acknowledgments

This work was supported by the National Natural Science Foundation of China (Grant No. 52231012) and the Hainan Provincial Natural Science Foundation of China (Grant No. 520MS071).

Appendix A. Detailed derivation of the governing equation process using Hamilton's principle

Integration on pipe x_1 and x_2 gives the total kinetic energy T of the system

$$T = 1/2\int_{x_1}^{x_2}\left\{m_p\left(\frac{\partial w}{\partial t}\right)^2 + m_f U^2\left(\frac{\partial w}{\partial x}\right)^2 + 2U\frac{\partial^2 w}{\partial t\partial x} + \left(\frac{\partial w}{\partial t}\right)^2 + \sum_{k=1}^{K}\left[m_k\left(\frac{\partial w(x_k,t)}{\partial t}\right)^2\right]\right\}dx \tag{A.1}$$

Integration on pipe x_1 and x_2 gives the total potential energy V of the system

$$V = 1/2\int_{x_1}^{x_2}\left\{EI\left(\frac{\partial^2 w}{\partial x^2}\right)^2 + (m_p + m_f)g(L-x)\left(\frac{\partial w}{\partial x}\right)^2 + \sum_{k=1}^{K}\left[m_k gH(x_k - x)\left(\frac{\partial w(x_k,t)}{\partial x}\right)^2\right]\right\}dx \tag{A.2}$$

Substituting Eqs. (A.1) and (A.2) into (7), the following equation is obtained

$$\begin{aligned}&\delta\int_{t_1}^{t_2}\int_{x_1}^{x_2} m_p\left(\frac{\partial w}{\partial t}\right)^2 + m_f\left[U^2\left(\frac{\partial w}{\partial x}\right)^2 + 2U\frac{\partial^2 w}{\partial t\partial x} + \left(\frac{\partial w}{\partial t}\right)^2\right] + \sum_{k=1}^{K}\left[m_k\left(\frac{\partial w(x_k,t)}{\partial t}\right)^2\right]\\ &- EI\left(\frac{\partial^2 w}{\partial x^2}\right)^2 - (m_p + m_f)g(L-x)\left(\frac{\partial w}{\partial x}\right)^2 - \sum_{k=1}^{K}\left[m_k gH(x_k - x)\left(\frac{\partial w(x_k,t)}{\partial x}\right)^2\right]dxdt = 0.\end{aligned} \tag{A.3}$$

Introducing of δ variables into the integral

$$\begin{aligned}&\int_{t_1}^{t_2}\int_{x_1}^{x_2}(m_p + m_f)\frac{\partial w}{\partial t}\delta\frac{\partial w}{\partial t} + m_f U^2\frac{\partial w}{\partial x}\delta\frac{\partial w}{\partial x} + 2m_f U\frac{\partial w}{\partial t}\delta\frac{\partial w}{\partial x} - EI\frac{\partial^2 w}{\partial x^2}\delta\frac{\partial^2 w}{\partial x^2}\\ &+ \sum_{k=1}^{K}\left[m_k\frac{\partial w(x_k,t)}{\partial t}\delta\frac{\partial w(x_k,t)}{\partial t}\right] - (m_p + m_f)g(L-x)\frac{\partial w}{\partial x}\delta\frac{\partial w}{\partial x}\\ &- \sum_{k=1}^{K}\left[m_k gH(x_k - x)\frac{\partial w(x_k,t)}{\partial x}\delta\frac{\partial w(x_k,t)}{\partial x}\right]dxdt = 0.\end{aligned} \tag{A.4}$$

Sub-integrate each term of Eq. (A.4) as follows For the first term:

$$\int_{t_1}^{t_2}\int_{x_1}^{x_2}(m_p + m_f)\frac{\partial w}{\partial t}\delta\frac{\partial w}{\partial t}dxdt \tag{A.5}$$

Eq. (A.4) switches the order of integration, first to the time integral before the length integral, and then to the divisional integral in the following

$$\int_{x_1}^{x_2}\int_{t_1}^{t_2}(m_p+m_f)\frac{\partial w}{\partial t}d(\delta w)dx=(m_p+m_f)\int_{x_1}^{x_2}\left[(\frac{\partial w}{\partial t}\delta w)_{t_1}^{t_2}-\int_{t_1}^{t_2}\frac{\partial^2 w}{\partial t^2}\delta w dt\right]dx \tag{A.6}$$

Since δw is equal to 0 at both ends of t_1 and t_2 on any path, it follows that

$$\int_{t_1}^{t_2}\int_{x_1}^{x_2}(m_p+m_f)\frac{\partial w}{\partial t}\delta\frac{\partial w}{\partial t}dxdt=-\int_{t_1}^{t_2}\int_{x_1}^{x_2}(m_p+m_f)\frac{\partial^2 w}{\partial t^2}\delta w dxdt \tag{A.7}$$

Similarly, δw is equal to 0 at both ends of x_1 and x_2 on any path the other terms can be derived as

For the second term:

$$\begin{aligned}&\int_{t_1}^{t_2}\int_{x_1}^{x_2}m_f U^2\frac{\partial w}{\partial x}\delta\frac{\partial w}{\partial x}dxdt=m_f U^2\int_{t_1}^{t_2}\int_{x_1}^{x_2}\frac{\partial w}{\partial x}d(\delta w)dt\\&=m_f U^2\int_{t_1}^{t_2}\left[(\frac{\partial w}{\partial x}\delta w)_{x_1}^{x_2}-\int_{x_1}^{x_2}\frac{\partial^2 w}{\partial x^2}\delta w dx\right]dt=-\int_{t_1}^{t_2}\int_{x_1}^{x_2}m_f U^2\frac{\partial^2 w}{\partial x^2}\delta w dxdt\end{aligned} \tag{A.8}$$

For the third term:

$$\begin{aligned}&\int_{t_1}^{t_2}\int_{x_1}^{x_2}2m_f U\frac{\partial w}{\partial t}\delta\frac{\partial w}{\partial x}dxdt=2m_f U\int_{t_1}^{t_2}\int_{x_1}^{x_2}\frac{\partial w}{\partial t}d(\delta w)dt\\&=2m_f U\int_{t_1}^{t_2}\left[(\frac{\partial w}{\partial t}\delta w)_{x_1}^{x_2}-\int_{x_1}^{x_2}\frac{\partial^2 w}{\partial t\partial x}\delta w dx\right]dt=-\int_{t_1}^{t_2}\int_{x_1}^{x_2}2m_f U\frac{\partial^2 w}{\partial t\partial x}\delta w dxdt.\end{aligned} \tag{A.9}$$

For the fourth term:

$$\begin{aligned}&\int_{t_1}^{t_2}\int_{x_1}^{x_2}\sum_{k=1}^{K}\left[m_k\frac{\partial w(x_k,t)}{\partial t}\delta\frac{\partial w(x_k,t)}{\partial t}\right]dxdt=\sum_{k=1}^{K}m_k\int_{x_1}^{x_2}\int_{t_1}^{t_2}\frac{\partial w(x_k,t)}{\partial t}d\delta w(x_k,t)dx\\&=\sum_{k=1}^{K}m_k\int_{x_1}^{x_2}\left[\left(\frac{\partial w(x_k,t)}{\partial t}\delta w(x_k,t)\right)_{t_1}^{t_2}-\int_{t_1}^{t_2}\frac{\partial^2 w(x_k,t)}{\partial t^2}\delta w(x_k,t)dt\right]dx\\&=-\int_{t_1}^{t_2}\int_{x_1}^{x_2}\sum_{k=1}^{K}m_k\frac{\partial^2 w(x_k,t)}{\partial t^2}\delta w(x_k,t)dxdt.\end{aligned} \tag{A.10}$$

For the fifth term:

$$\begin{aligned}&-\int_{t_1}^{t_2}\int_{x_1}^{x_2}EI\frac{\partial^2 w}{\partial x^2}\delta\frac{\partial^2 w}{\partial x^2}dxdt=-EI\int_{t_1}^{t_2}\int_{x_1}^{x_2}\frac{\partial^2 w}{\partial x^2}d\delta\frac{\partial w}{\partial x}dt\\&=-EI\int_{t_1}^{t_2}\left[\left(\frac{\partial^2 w}{\partial x^2}d\delta\frac{\partial w}{\partial x}\right)_{x_1}^{x_2}-\int_{x_1}^{x_2}\frac{\partial^3 w}{\partial x^3}\delta\frac{\partial w}{\partial x}dx\right]dt=EI\int_{t_1}^{t_2}\int_{x_1}^{x_2}\frac{\partial^3 w}{\partial x^3}\delta\frac{\partial w}{\partial x}dxdt\\&=EI\int_{t_1}^{t_2}\int_{x_1}^{x_2}\frac{\partial^3 w}{\partial x^3}(d\delta w)dt=EI\int_{t_1}^{t_2}\left[\left(\frac{\partial^3 w}{\partial x^3}\delta w\right)_{x_1}^{x_2}-\int_{x_1}^{x_2}\frac{\partial^4 w}{\partial x^4}\delta w dx\right]dt\\&=-EI\int_{t_1}^{t_2}\int_{x_1}^{x_2}\frac{\partial^4 w}{\partial x^4}\delta w dxdt.\end{aligned} \tag{A.11}$$

For the sixth term:

$$\begin{aligned}
&-\int_{t_1}^{t_2}\int_{x_1}^{x_2}(m_p+m_f)g(L-x)\frac{\partial w}{\partial x}\delta\frac{\partial w}{\partial x}dxdt\\
&=-(m_p+m_f)gL\int_{t_1}^{t_2}\int_{x_1}^{x_2}\frac{\partial w}{\partial x}(d\delta w)dt+(m_p+m_f)g\int_{t_1}^{t_2}\int_{x_1}^{x_2}x\frac{\partial w}{\partial x}(d\delta w)dt\\
&=-(m_p+m_f)gL\int_{t_1}^{t_2}\left[\left(\frac{\partial w}{\partial x}\delta w\right)_{x_1}^{x_2}-\int_{x_1}^{x_2}\frac{\partial^2 w}{\partial x^2}\delta w dx\right]dt+(m_p+m_f)g\int_{t_1}^{t_2}[\left(x\frac{\partial w}{\partial x}\delta w\right)_{x_1}^{x_2}\\
&-\int_{x_1}^{x_2}\left(\frac{\partial w}{\partial x}+x\frac{\partial^2 w}{\partial x^2}\right)\delta w dx]dt=\int_{t_1}^{t_2}\int_{x_1}^{x_2}(m_p+m_f)gL\frac{\partial^2 w}{\partial x^2}\delta w dxdt\\
&-(m_p+m_f)g\int_{t_1}^{t_2}\int_{x_1}^{x_2}\frac{\partial w}{\partial x}\delta w dxdt-(m_p+m_f)g\int_{t_1}^{t_2}\int_{x_1}^{x_2}x\frac{\partial^2 w}{\partial x^2}\delta w dxdt\\
&=\int_{t_1}^{t_2}\int_{x_1}^{x_2}(m_p+m_f)g(L-x)\frac{\partial^2 w}{\partial x^2}\delta w dxdt-\int_{t_1}^{t_2}\int_{x_1}^{x_2}(m_p+m_f)g\frac{\partial w}{\partial x}\delta w dxdt
\end{aligned}\tag{A.12}$$

For the seventh term:

$$\begin{aligned}
&-\int_{t_1}^{t_2}\int_{x_1}^{x_2}\sum_{k=1}^{K}m_k gH(x_k-x)\frac{\partial w(x_k,t)}{\partial x}\delta\frac{\partial w(x_k,t)}{\partial x}dxdt=-\sum_{k=1}^{K}m_k gH(x_k-x)\int_{t_1}^{t_2}\int_{x_1}^{x_2}\frac{\partial w(x_k,t)}{\partial x}d(\delta w(x_k,t))dt\\
&=-\sum_{k=1}^{K}\left[m_k gH(x_k-x)\int_{t_1}^{t_2}\left(\frac{\partial w(x_k,t)}{\partial x}\delta w(x_k,t)\right)_{x_1}^{x_2}-\int_{x_1}^{x_2}\frac{\partial^2 w(x_k,t)}{\partial x^2}\delta w(x_k,t)dx\right]dt\\
&=\int_{t_1}^{t_2}\int_{x_1}^{x_2}\sum_{k=1}^{K}m_k gH(x_k-x)\frac{\partial^2 w(x_k,t)}{\partial x^2}\delta w(x_k,t)dxdt
\end{aligned}\tag{A.13}$$

In summary, By substituting Eqs. (A.7)–(A.13) into Eq. (A.4), the vibration equation is given as

$$\begin{aligned}
&\int_{t_1}^{t_2}\int_{x_1}^{x_2}[EI\frac{\partial^4 w}{\partial x^4}+m_f U^2\frac{\partial^2 w}{\partial x^2}+2m_f U\frac{\partial^2 w}{\partial x\partial t}+(m_p+m_f)\frac{\partial^2 w}{\partial t^2}+\sum_{k=1}^{K}m_k\frac{\partial^2 w(x_k,t)}{\partial t^2}\\
&-(m_p+m_f)g(L-x)\frac{\partial^2 w}{\partial x^2}+(m_p+m_f)g\frac{\partial w}{\partial x}-\sum_{k=1}^{K}m_k gH(x_k-x)\frac{\partial^2 w(x_k,t)}{\partial x^2}]\delta w dxdt=0.
\end{aligned}\tag{A.14}$$

Appendix B. Weighting coefficient factor for HDQ method

The weighting coefficients of the first derivative $A_{ij}^{(1)}$ and second derivatives $A_{ij}^{(2)}$ for $i \neq j$ is given by

$$A_{ij}^{(1)}=\frac{\pi P(x_i)/2}{P(x_j)\sin[\pi(x_i-x_j)/2]}\quad i,j=1,2\ldots N,\tag{B.1}$$

$$A_{ij}^{(2)}=A_{ij}\left[2A_{ii}^{(1)}-\pi\cot\left(\frac{x_i-x_j}{2}\right)\pi\right],\tag{B.2}$$

with

$$P(x_i)=\prod_{j=1,j\neq i}^{N}\sin\left(\frac{x_i-x_j}{2}\pi\right).\tag{B.3}$$

The weighting coefficients of the first and second derivatives $A_{ij}^{(n)}$ for $i=j$ are defined as

$$A_{ii}^{(n)}=-\sum_{j=1,j\neq i}^{N}A_{ij}^{(n)},\ n=1,2.\tag{B.4}$$

The weighting coefficients for high derivatives are thereby expressed as

$$A_{ij}^{(n)}=\sum_{k=1}^{N}A_{ik}^{(1)}A_{kj}^{(n-1)}.\tag{B.5}$$

References

Addessi, D., Lacarbonara, W., Paolone, A., 2005. Free in-plane vibrations of highly buckled beams carrying a lumped mass. J. Fluids Struct. 180, 133–156.
Askarian, A.R., Permoon, M.R., Shakouri, M., 2020. Vibration analysis of pipes conveying fluid resting on a fractional Kelvin-Voigt viscoelastic foundation with general boundary conditions. Microfluid Nanofluidics 179, 105702.
Bahaadini, R., Dashtbayazi, M.R., Hosseini, M., Khalili-Parizi, Z., 2018. Stability analysis of composite thin-walled pipes conveying fluid. Ocean Eng. 160, 311–323.
Balkaya, M., Kaya, M.O., 2021. Analysis of the instability of pipes conveying fluid resting on two-parameter elastic soil under different boundary conditions. Ocean Eng. 241, 110003.
Bert, C.W., Malik, M., 1996. Free vibration analysis of thin cylindrical shells by the differential quadrature method. J. Press. Vessel Technol. 118 (1), 1–12.
Butt, M.F.J., Paidoussis, M.P., Nahon, M., 2021. Dynamics of a confined pipe aspirating fluid and concurrently subjected to external axial flow: An experimental investigation. J. Fluids Struct. 104, 103299.
Copeland, G.S., Moon, F.C., 1992. Chaotic flow-induced vibration of a flexible tube with end mass. J. Fluids Struct. 6, 705–718.
ElNajjar, J., Daneshmand, F., 2020. Stability of horizontal and vertical pipes conveying fluid under the effects of additional point masses and springs. Ocean Eng. 206, 1–15.
Fazelzadeh, S.A., Kazemi-Lari, M.A., 2013. Stability analysis of partially loaded Leipholz column carrying a lumped mass and resting on elastic foundation. J. Sound Vib. 332, 595–607.
Hill, J.L., Swanson, C.P., 1970. Effects of lumped masses on the stability of fluid conveying tubes. Int. J. Appl. Mech. 37, 494–497.
Hisamatsu, R., Utsunomiya, T., 2023. Free vibration and stability of a fully submerged pipe aspirating water: An experiment and new physical insights. J. Fluids Struct. 116, 103789.
Kheiri, M., Paidoussis, M.P., 2015. Dynamics and stability of a flexible pinned-free cylinder in axial flow. J. Fluids Struct. 55, 204–217.
Khudayarov, B.A., Komilova, K.M., Turaev, F.Z., Aliyarov, J.A., 2020. Numerical simulation of vibration of composite pipelines conveying fluids with account for lumped masses. Int. J. Press. Vessel. Pip. 179, 104034.
Kuiper, G.L., Metrikine, A.V., 2005. Dynamic stability of a submerged, free-hanging riser conveying fluid. J. Fluids Struct. 280 (3-5), 1051–1065.
Kuiper, G.L., Metrikine, A.V., 2008. Experimental investigation of dynamic stability of a cantilever pipe aspirating fluid. J. Fluids Struct. 24 (4), 541–558.
Li, Y.D., Yang, Y.R., 2017. Vibration analysis of conveying fluid pipe via He's variational iteration method. Appl. Math. Model. 43, 409–420.
Li, M., Zhao, X., Li, X., Chang, X.P., Li, Y.H., 2018. Stability analysis of oil-conveying pipes on two-parameter foundations with generalized boundary condition by means of Green's functions. Eng. Struct. 173, 300–312.
Liang, X., Zha, X., Jiang, X., Wang, L.Z., Leng, J.X., Cao, Z., 2018. Semi-analytical solution for dynamic behavior of a fluid-conveying pipe with different boundary conditions. Ocean Eng. 163, 183–190.
Ma, Y.Q., You, Y.X., Chen, K., Hu, L.L., Feng, A.C., 2023. Application of harmonic differential quadrature (HDQ) method for vibration analysis of pipes conveying fluid. Appl. Math. Comput. 439, 127613.
Modarres-Sadeghi, Y., Semler, C., Wadham-Gagnon, M., Paidoussis, M.P., 2007. Dynamics of cantilevered pipes conveying fluid. Part 3: three-dimensional dynamics in the presence of an end-mass. J. Fluids Struct. 23, 589–603.
Na, K.S., Kim, J.H., Park, J.S., 2019. Dynamic stability analyses of the liquid–filled cylindrical shells with lumped masses under a follower force. Int. J. Aeronaut. Space Sci. 20, 664–672.
Paidoussis, M.P., 1970. Dynamics of tubular cantilevers conveying fluid. J. Mech. Eng. Sci. 12 (2), 85–103.
Paidoussis, M.P., 2008. Dynamics of a long tubular cantilever conveying fluid downwards, which then flows upwards around the cantilever as a confined annular flow. J. Fluids Struct. 24, 111–128.
Paidoussis, M.P., 2014. Fluid-Structure Interactions: Slender Structures and Axial Flow, Vol. 1. Academic press, London.
Paidoussis, M.P., 2016. Fluid-Structure Interactions: Slender Structures and Axial Flow, Vol. 2. Academic press, London.
Paidoussis, M.P., 2022. Pipes conveying fluid: A fertile dynamics problem. J. Fluids Struct. 114, 103664.
Rinaldi, S., Paidoussis, M.P., 2010. Dynamics of a cantilevered pipe discharging fluid, fitted with a stabilizing end-piece. J. Fluids Struct. 26 (3), 517–525.
Wadham-Gagnon, M., Paidoussis, M.P., 2013. Chaotic oscillations of long pipes conveying fluid in the presence of a large end-mass. Comput. Struct. 122, 192–201.
Yamashita, K., Kitaura, K., Nishiyama, N., Yabuno, H., 2022. Non-planar motions due to nonlinear interactions between unstable oscillatory modes in a cantilevered pipe conveying fluid. Mech. Syst. Signal Process. 178, 109183.
Yi, H.R., Zhou, K., Dai, H.L., Wang, L., Ni, Q., 2020. Study on stability and modal evolution characteristics of the cantilevered fluid-conveying pipe attached with the lumped mass. J. Theoret. Appl. Mech. 52 (6), 1800–1810.
Yoon, H.I., Son, I.S., 2007. Dynamic response of rotating flexible cantilever pipe conveying fluid with tip mass. Int. J. Mech. Sci. 49 (7), 878–887.
Zhang, T., Ouyang, H., Zhang, Y.O., Lv, B.L., 2016. Nonlinear dynamics of straight fluid-conveying pipes with general boundary conditions and additional springs and masses. Appl. Math. Model. 40, 7880–7900.
Zhen, W., Zou, L., 2022. Natural frequency analysis of deep-sea mining riser considering varying tension and buffer station. Ocean Eng. 264, 112372.